Modulation of rotation-induced lift force for cell filtration in a low aspect ratio microchannel

Jian Zhou,[1] Premkumar Vummidi Giridhar,[2] Susan Kasper,[2] and Ian Papautsky[1,a)]
[1]*BioMicroSystems Lab, Department of Electrical Engineering and Computing Systems, University of Cincinnati, Cincinnati, Ohio 45221, USA*
[2]*Department of Environmental Health, College of Medicine, University of Cincinnati, Cincinnati, Ohio 45221, USA*

(Received 18 May 2014; accepted 18 July 2014; published online 30 July 2014)

Cell filtration is a critical step in sample preparation in many bioapplications. Herein, we report on a simple, filter-free, microfluidic platform based on hydrodynamic inertial migration. Our approach builds on the concept of two-stage inertial migration which permits precise prediction of microparticle position within the microchannel. Our design manipulates equilibrium positions of larger microparticles by modulating rotation-induced lift force in a low aspect ratio microchannel. Here, we demonstrate filtration of microparticles with extreme efficiency (>99%). Using multiple prostate cell lines (LNCaP and human prostate epithelial tumor cells), we show filtration from spiked blood, with 3-fold concentration and >83% viability. Results of a proliferation assay show normal cell division and suggest no negative effects on intrinsic properties. Considering the planar low-aspect-ratio structure and predictable focusing, we envision promising applications and easy integration with existing lab-on-a-chip systems. © *2014 AIP Publishing LLC*.
[http://dx.doi.org/10.1063/1.4891599]

INTRODUCTION

Microfluidic platforms for separation and filtration of bioparticles have been gaining prominence due to their superior performance. A variety of membrane-free and label-free microfluidic systems have been reported using acoustic,[1,2] electric,[3] dielectric,[4,5] magnetic,[6,7] optical,[8] and hybrid[9–11] forces. These devices are based on the physical and morphological properties of target sample (e.g., cell size) and generally offer high filtration efficiency ($\eta > 90\%$). However, the sophisticated control of external forces on these platforms increases system complexity and cost, making them less practical. Further, throughput of such systems is often low due to the need to expose sample to the force field.[12] Recent developments in inertial microfluidics have the potential to overcome these challenges.

Inertial microfluidic approaches manipulate hydrodynamic forces acting on bioparticles to achieve lateral displacement by modulating channel geometry. Microparticles flowing in a microchannel experience a shear-induced lift force (F_s) due to parabolic velocity profile of Poiseuille flow.[13] This force drives particles away from the microchannel center and toward the channel walls. As particles migrate laterally to the wall, an opposing wall-induced lift force (F_w) pushes particles away due to change in vorticity around the particle surface.[13] It is the resulting net force that generates particle equilibrium in distinct positions within the channel cross-section. In a round channel, the interaction of these forces results in the "Segré annulus" at $\sim 0.2D_h$ (hydraulic diameter) away from the walls, which was first observed in 1960s.[14,15] This distance was found to decrease with increasing flow Reynolds number (Re).[16,17] In radially

a)Author to whom correspondence should be addressed. Electronic mail: ian.papautsky@uc.edu. Tel.: 513-556-2347. Fax: 513-556-7326.

asymmetric channels (e.g., square or rectangular cross-section), another small but critical force due to particle rotation dictates particle motion near sidewalls.[13] This rotation-induced lift force (F_Ω) causes cross-lateral migration that leads to a reduced number of equilibrium positions, four in a square channel[18,19] and two in a rectangular channel.[13] In a curved channel, due to addition of the Dean force, the equilibrium positions can be further reduced to one.[20,21] Since the inertial forces are strongly dependent on particle diameter (a), discovery of distinct focusing positions has triggered the burgeoning of techniques for size-selective separation and filtration of particles and cells in simple microchannels with various geometries.[22–31]

Particle and cell filtration in straight, rectangular microchannels have been successfully demonstrated by a number of groups. For example, we showed filtration of 7.32 μm diameter particles from smaller particles ($a = 1.9\,\mu$m) in a high aspect-ratio (AR $= h/w > 1$, where h is height and w is width) channel.[32,33] Mach and Di Carlo[34] further demonstrated filtration of red blood cells (RBCs) from bacteria at high throughput (200 μl/min) in a similar design. A higher throughput ($\sim$8 ml/min) and efficiency ($\eta = 90\%$) were achieved in their massively paralleled 256-channel system.[34] In a low AR (AR < 1) straight microchannel, Hansson *et al.* demonstrated an even higher efficiency ($\eta > 95\%$) using 10 μm diameter particles.[35] In terms of collecting large cells, a low AR channel is preferred as the target cells can be collected from a single central outlet, rather than from the two side outlets as in high AR microchannels. While these systems offer good performance in filtration of particles, parameters that are critical in downstream cell analysis, such as viability and proliferation of collected cells, are yet to be explored.

In this work, we report on an approach for cell filtration in a low-AR rectangular microchannel with improved performance. Our design is based on the model of two-stage inertial migration (Fig. 1(a)),[13] where randomly distributed particles first migrate to the top and bottom faces of the channel dominated by F_s in the first fast stage and migrate transversely toward their two equilibrium positions undergoing F_Ω in the second slow stage.[13] Since lateral migration velocity is strongly dependent on cell size ($U_L \propto a^2$ in stage 2),[13] larger cells complete both stages of migration and achieve equilibrium much faster than the smaller ones. Placing a trifurcating outlet following the full equilibrium of larger cells leads to an easy removal of smaller cells (or cell-free volume for single cell species), as illustrated in Fig. 1(b). Our results with LNCaP (lymph node carcinoma of prostate) and HPET (human prostate epithelial tumor) cells show that large cells can be successfully collected from the central outlet of the device with an extremely high efficiency ($\eta = 99.5\%$), with no cells found in side outlets. The 67% of the smaller cells are removed in a single pass, resulting in 3$\times$ enhancement of target cell purity; additional passes can offer an even higher enhancement. Cell viability was at 83% and the collected cells divided normally during the proliferation tests. This filtration approach suggests that sample concentration (for single cell species) is possible in a flow-through microfluidic system, which typically requires multiple centrifugation and resuspension steps on the macroscale. Ultimately, coupled with separation channels, this approach can offer an attractive alternative in the area of microfluidic sample preparation.

RESULTS

Particle focusing and filtration

We optimized and validated our microfluidic filtration device design using fluorescent polystyrene beads before proceeding to experiments with cells. In the device, randomly dispersed particles at the inlet rapidly migrate to the top and bottom faces and progressively form three streams at $Re = 120$, as observed from the top in Fig. 2. Particles in the corner streams gradually migrate toward the width centers and finally disappear at downstream length of $L = 12$ mm, indicating completion of the two-stage migration process. The result is the two face-centered focusing positions. To observe focusing of microparticles from sides, we used a high-AR channel of the same dimensions. This is an approach we used in the past[13] and it allowed us to visualize two focusing positions near top and bottom of the low-AR channel (Fig. 2(c)). Based on these observations, a complete picture of the focusing

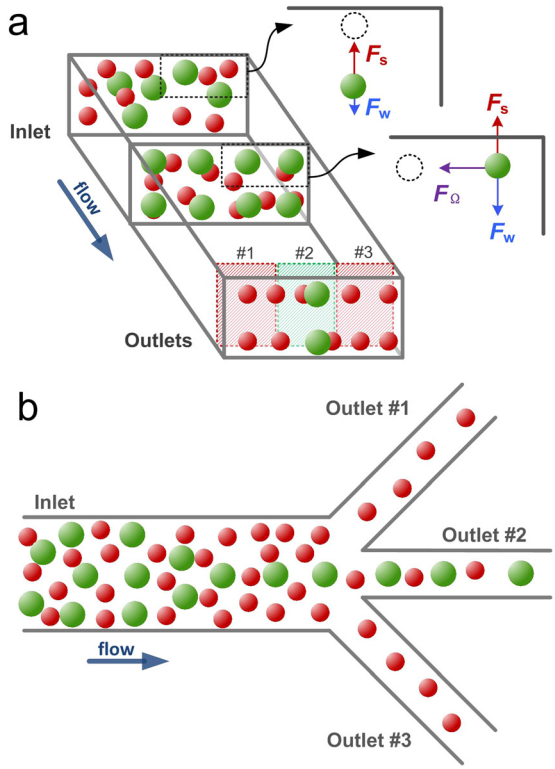

FIG. 1. Schematic (a) and device layout (b). Particles flowing in a low aspect-ratio microchannel first migrate to top and bottom walls undergoing a shear-induced lift force F_S (stage 1); once the shear-induced lift force balances with a wall-induced lift force F_W, particles further migrate toward the centers of horizontal walls experiencing a rotation-induced lift force F_Ω (stage 2). Due to the strong size-dependent migration velocity, the larger particles complete the two-stage migration and equilibrate to the two long-face-centered positions much faster than the smaller particles. By setting the channel length to the focusing length of the larger particles, they can be filtered from the smaller particles through the central outlet.

positions in a low-AR microchannel emerges, confirming presence of two face-centered focusing positions near the top and bottom.

We experimentally measured focusing lengths of four particles ranging from 7.32 μm to 20 μm in diameter as a function of Re. For this, linescans of fluorescent intensity at progressive downstream positions were obtained (Fig. 3(a)), and full width at tenth maximum (FWTM) for each was plotted as a function of the measurement position. As results in Fig. 3(b) for 20 μm diameter particles in a 100 μm $\times$ 50 μm ($w \times h$) channel show, the FWTM values ultimately stabilize when full focusing is achieved. The downstream length at which this stabilization occurs is considered as focusing length for a given flow condition. As expected, Fig. 3(b) shows that for the focusing length L becomes longer with increasing Re.

The experimental results can also be confirmed through direct calculation using the model of two-stage migration. In a low-AR channel with hydraulic diameter D_h, focusing length L is given by[13]

$$L = \frac{3\pi\mu D_h^2}{4\rho U_f a^3}\left(\frac{h}{C_L^-} + \frac{w}{C_L^+}\right), \tag{1}$$

where μ and ρ are the dynamic viscosity and density of the carrier fluid, U_f is the average flow velocity, and $D_h = 2hw/(h+w)$. The negative and positive lift coefficients ($C_L{}^-$ and $C_L{}^+$, respectively) were estimated in our recent work.[13] Results in Fig. 3(c) show that both experimental and theoretical data are in strong agreement, validating Eq. (1) for use with low AR microchannels. Following this validation, we designed a 10 mm long channel for filtration of 20 μm diameter particles (or cells) using flows in the $15 < Re < 100$ range.

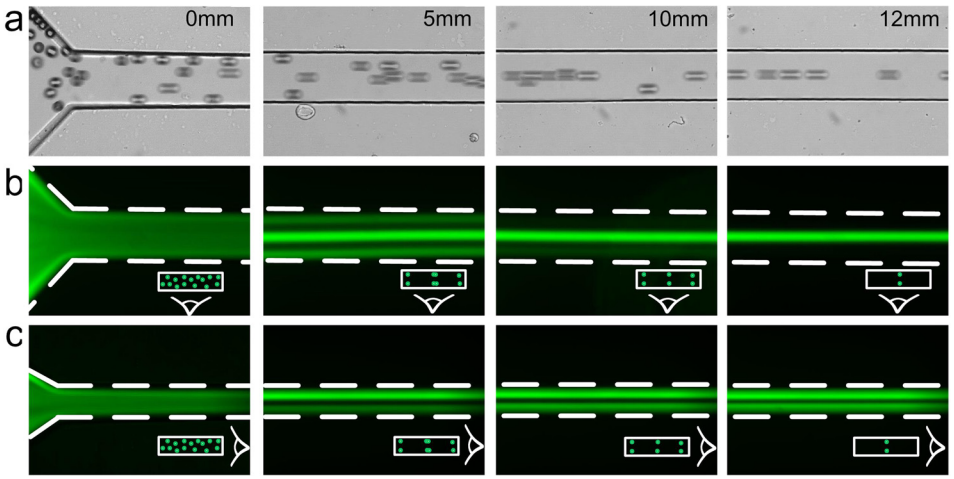

FIG. 2. Demonstration of two-position focusing at $Re = 120$ in a 100 μm × 50 μm microchannel. Topview of bright field (a) and corresponding fluorescent (b) images show the evolution of particle streams in a rectangular microchannel. (c) Corresponding images of sideview at progressive downstream positions. The polystyrene particles were 20 μm in diameter.

Prior to cell filtration, a mixture of polystyrene particles was used to validate the filtration concept. As results in Fig. 4(a) show, larger particles (yellow fluorescent stream in inset) focus in the middle of the channel and exit through the central outlet. The smaller 7.32 μm diameter particles (green fluorescence in inset) remained unfocused and evenly distributed among all three outlets, which is expected since their focusing length (~60 mm) is much longer than the channel length (10 mm) (based on Eq. (1) and data in Fig. 3(c)). Quantitative counting of collected particles confirmed that smaller particles are uniformly distributed and showed that nearly all 20 μm diameter particles exited through the middle outlet. The filtration efficiency was calculated to be approximately $\eta = 99.5\%$, with coefficient of variation $CV = 0.93\%$ ($n = 5$). This result illustrates a 3× enrichment in concentration and purity of 20 μm diameter particles through removal of 2/3 of smaller particles. The high filtration efficiency and the reduced volume (1/3 of the injected volume) are especially promising in the applications of sample concentration.

To further demonstrate feasibility of cell filtration, we spiked blood with 20 μm diameter microparticles. The brightfield image in Fig. 4(c) shows particles and uniformly dispersed blood cells (mostly RBCs) at inlet. At the outlet at 10 mm downstream (Fig. 4(d)), as expected all particles exited through the center outlet after focusing into the single stream, while RBCs were observed to be evenly distributed and behave similar to the 7.32 μm diameter particles (regardless their non-spherical shape).

Cell filtration

To demonstrate the potential for cell filtration, we used LNCaP cells due to their great relevance. Prostate cancer is the most frequent form of cancers in males in most western countries;[36] an estimation of 1 in 6 men in the US is diagnosed with prostate cancer.[37,38] However, the mechanism of development and progression remain poorly understood.[37,38] One of the contributing factors is the challenge of filtering these cells from mixtures, which we hope to alleviate in this work.

A suspension of LNCaP cells (2500 cells/ml) was introduced into the device at $Re = 50$. The mature LNCaP cells are approximately 21 μm in diameter in suspension and thus behave similar to the 20 μm diameter particles when introduced into our microfluidic channel. As brightfield images in Fig. 5(a) show, the uniformly dispersed LNCaP cells progressively order

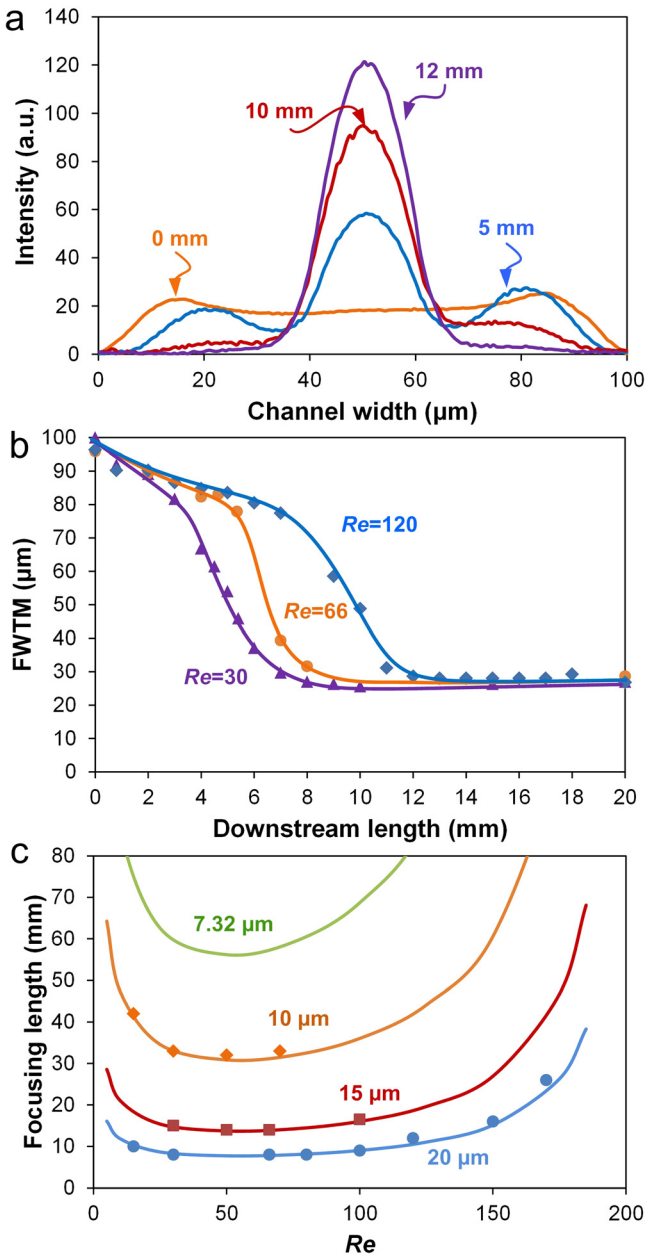

FIG. 3. Measurements of focusing length. (a) Fluorescent intensity line scans across channel width at consecutive downstream positions. (b) FWTM of major peaks as a function of downstream length at various *Re*. (c) Focusing length as a function of *Re*. The prediction curves were calculated based on two-stage migration model. Solid symbols indicate experimental measurements. All data were obtained using polystyrene beads (10 μm, 15 μm, and 20 μm in diameter) in a 100 μm $\times$ 50 μm microchannel.

into a single stream in the middle at the channel. As flow increased to $Re = 70$, cells were also observed in the side outlets, reducing the efficiency to ~72%. Equal number of cells ($\eta = 33\%$) were observed at higher *Re*, indicating that no cell filtration occurred.

The observed decrease in filtration efficiency at $Re > 50$ is primarily due to the limited channel length. According to Fig. 3(c) and Eq. (1), the focusing length becomes longer as *Re* increases above 40. At $Re = 50$, the focusing length of $a = 20\,\mu$m particles was $L \sim 8.5$ mm. But at $Re = 100$, $L > 10$ mm, which is insufficient for cells to focus completely into a single stream in our device. A longer microchannel would be necessary to ensure high filtration efficiency at

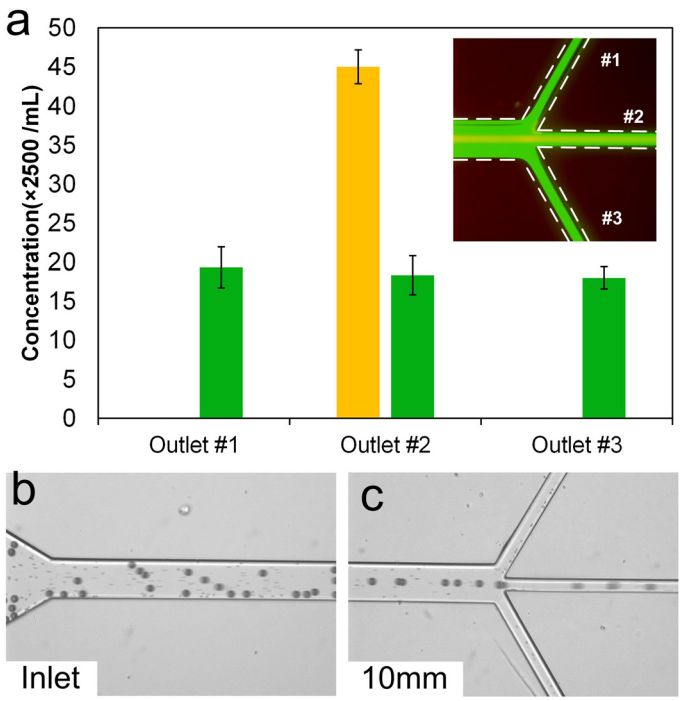

FIG. 4. Demonstration of size-selective filtration at $Re = 50$. (a) Filtration of 20 μm diameter particles from a mixture with 7.32 μm diameter particles. Large particles (yellow stream in the inset) were collected through the central outlet, while smaller particles (green in the inset) were evenly distributed in all three outlets. Error bars represent standard deviations of three counts. (b) Bright field image of the inlet illustrating suspension of 20 μm particles spiked in blood. Small dots in the channel are blood cells. (c) Particles exiting through the central outlet and RBCs exiting through every outlet.

faster flows. In addition, the inherent size variation of cells also exhibits a stronger influence at higher *Re*, with the slightly smaller cells needing a considerable longer channel to focus ($\Delta L/\Delta a \sim a^{-3}$).[13]

Similar to efficiency, a downward trend of filtration viability was observed as *Re* increased (Fig. 5(c)). We used trypan blue exclusion test to identify viable cells in the collected sample.

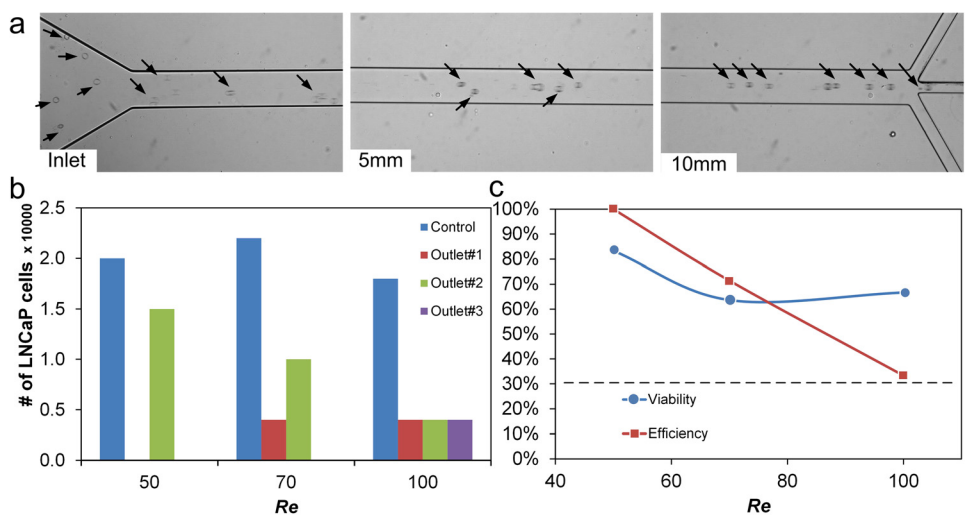

FIG. 5. Validation of cell focusing in the microchannel. (a) Bright field images showing development of LNCaP cell train at different downstream positions at $Re = 50$. (b) Cells collected at each outlet at three *Re*. Control represents the cells collected without passing through the device. (c) Efficiency and viability data for a 10 mm long microchannel.

A viability of 83.3% was achieved at $Re = 50$ for a single-stage process. At higher Re with faster flow, the increased shear stress reduced cell viability even further, with approximately 1/3 of cells being damaged at $Re > 100$.

Although the circulating tumor cells (CTCs) in blood stream can transiently experience the shear stress as high as 3000 dyn/cm^2,[39] a significant loss of cancer cell viability can occur at shear stress levels above 100 dyn/cm^2. The maximum shear stress near wall (τ_w) of a channel flow can be calculated using Poiseuille's Law as

$$\tau_w = \frac{32\mu Q}{\pi D_h^3}, \tag{2}$$

where Q is the volumetric flow rate. In this work, at $Re = 50$, the shear stress is calculated to be $\tau_w = 128$ dyn/cm^2. While the shear in the main channel can be the cause of cell loss, the reduced viability is most likely the result of the much smaller outlet branches ($w = 32\,\mu$m) where $\tau_w = 199$ dyn/cm^2 despite only 1/3 of the input flow rate. The dependence of cell viability on shear stress we find here is similar to the work by Barnes *et al.*[39] using prostate cells (PC-3). Nevertheless, 83% viability is sufficiently high considering the fragile nature of the LNCaP cells.

We carried out proliferation assays to determine whether the hydrodynamic filtration affects the intrinsic properties of cells (Fig. 6). The unaffected proliferation and the ability to be re-cultured are crucial for downstream analysis. The number of viable cells (based on trypan blue staining) was counted every 24 h for 5 days subsequent to processing in the device. The coincidence of the two curves in Fig. 6 suggests that cell proliferation was unaffected. No significant immediate or long term (5 days) effects could be detected in the LNCaP cells subjected to filtration compared to the untreated control.

To further demonstrate filtration of cancer cells, we used spiked blood with human prostate epithelial tumor (HPET). HPET cells are derived from a high grade (Gleason 9) prostate punch biopsy and recapitulate the histopathology of human prostate cancer *in vivo*.[40–42] The HPET cells are 18–22 μm in diameter in suspension and were spiked at concentration of 2500 cells/ml into diluted blood (~0.5% hematocrit). The HPET cells were stained with green live cell tracker dye (ER-Tracker^{TM} Green, Invitrogen) to permit visualization. While the brightfield image in Fig. 7(a) reveals that the RBCs are everywhere, similar to smaller particles in Fig. 4(b), the corresponding fluorescent image in Fig. 7(b) indicates that the HPET cells entrained in the middle and exited from the central outlet analogous to 20 μm diameter particles and LNCaP

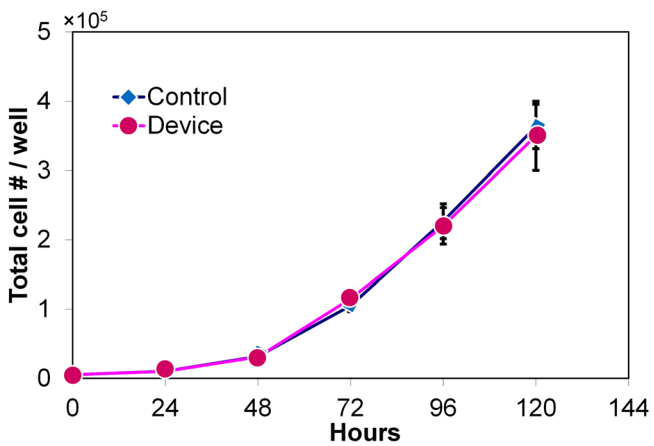

FIG. 6. Proliferation results illustrating the LNCaP cell population that was filtered in the device vs. control population. The control sample consisted of cells that did not pass through the device. The error bars represent one standard deviation of independent three measurements.

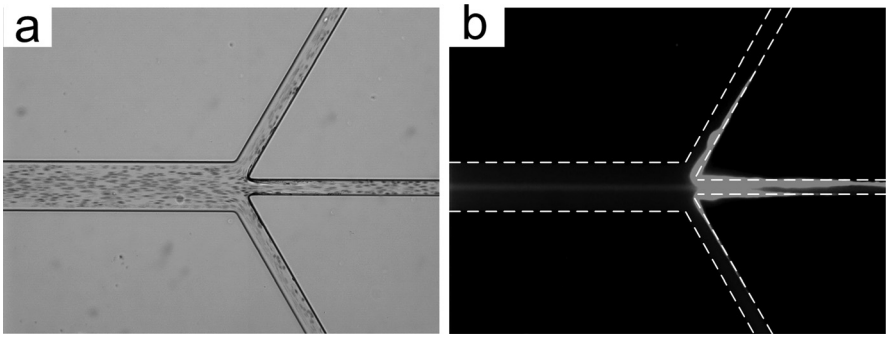

FIG. 7. Filtration of HPET cells from blood at $Re = 50$. (a) Brightfield image illustrating cells (mostly RBCs) in the microchannel. (b) Corresponding fluorescent image illustrating a stream of HPET cells in the middle of the channel.

cells used previously. Cell debris was observed at the channel walls at trifurcation, resulting in excessive shear stress which can be the primary contributor to cell loss during processing. Nonetheless, filtration of cancer cells from the mixture has been successfully demonstrated.

DISCUSSION

The excellent filtration efficiency (~99%) of our device permits concentration of sample for biological, biomedical, and possibly environmental applications.[43–46] Conventionally, centrifuge is one of the most common instruments in these laboratory settings for sample preparation, which typically requires multiple steps of centrifugations and re-suspensions. This process is usually time-consuming and laborious.[43] Our microfluidic platform potentially overcomes such limitation. As demonstrated in this work, every large particle and cells injected into the channel were collected from the target outlet, while 2/3 of the initial volume was fractioned from side outlets. These results suggest a 3-fold increase in concentration of the collected particles.

Since the volume fraction (VF) in the target outlet can be tuned by the resistance of each outlet channel, we can increase concentration of the filtered sample using different outlet systems. Since flow resistance R for a channel of length L is defined as $R = 128\,\mu L/\pi D_h^4$, it is possible to alter flow fraction by either increasing the channel length L or decreasing the channel width w (and thus hydraulic diameter D_h). For instance, a 2:1:2 ratio of the three outlet channel width will offer a 7.3× increase in target concentration. Similarly, a 1:2:1 ratio of the three outlet channel length will provide a 5× enhancement in target concentration. With further optimization, even higher concentration enhancement should be possible. The resistances of side outlets, however, should be balanced to avoid disturbing particle focusing and to ensure collection from the central outlet.

Considering the high throughput (225 μl/min for single channel) nature of the described inertial microfluidic device, such sample concentration can be very time-efficient. In a chip with 10 parallel channels, processing a 10 ml of sample takes <4.5 min and does not require repeated centrifugation steps. Ultimately, the approach can be automated. Although the focus of the current paper is on 20 μm diameter particles, the platform is generally applicable to other particle/cell sizes based on our model of two-stage migration.[13]

Performance characteristics of our device are comparable, and in some cases exceed that of the existing microfluidic cell filtration approaches, which are summarized in Table I. Our efficiency is comparable to the active microfluidic platforms, such as those relying on dielectrophoretic or acoustic methods which generally require additional steps or complex control circuitry. Deterministic lateral displacement (DLD) and non-inertial approaches have demonstrated similar filtration performance, but at considerably lower throughput. While Liu *et al.*[47] reported a high-throughput (2 ml/min) version of the DLD approach, no cell viability data were reported, despite the fact that high flow rates can deform cells, altering their morphology and viability.

As Table I shows, flow rates used in our device are in the middle of the range of other inertial based platforms, which permits very high filtration efficiency while maintaining relatively

TABLE I. Performance of recent cell filtration platforms. DLD is deterministic lateral displacement; vDLD is virtual DLD; ER is the enrichment ratio. Some flow rate data were converted from other parameters in the corresponding references.

Technique	Sample	Flow rate (μl/min)	Efficiency	Viability	ER	Remarks	References
Dielectrophoretic	Rare bacteria	5	95%		200	Buffer required	55
	MDA-MB cancer	20	70%–80%			Buffer required	56
Immunoselection	H1650 cancer	167	96%			Magnetic	57
	CTC	16–32	65%	98%	10^6	microchip	58
Acoustic	Prostate cancer	100	73%–94%			Nonfixed, buffer	59
	MCF-7	67	91%			Buffer required	60
DLD/vDLD	MCF-7	2000	99%		115	DLD	47
	Polystyrene particles	4.1	>97%			vDLD, buffer	61
Inertial	Bacteria in blood	200			4	Two stages	34
	MCF-7	4000	<27%	86%	10^4	Vortex, 8 channels	48
	Leukocyte	800	>80%	98%		Trapezoid spiral	49
	Malaria infected RBCs	5	>80%		2	Deformability	50
	MCF-7	5	99%			Sheath flow	52
	MCF-7/modMCF-7	42		92%	5.35	Deformability	51
	Neuroblastoma and glioma	2500	>80%	90%		Dean flow, spiral	21
	LNCaP, HPET	225	>99.5%	83%	3	Single stage	This work
Non-inertial	MV3-melanoma	0.33	98.7%			Sheath flow	62

high throughput. Although recent work by Sollier *et al.*[48] reported a high flow rate of 4 ml/min, it was achieved in 8 channels with a footprint 80× larger than that of our channel. We can readily package over 40 parallel channels within a similar chip size, which theoretically would lead to a throughput of 9 ml/min. Wu *et al.*[49] showed >80% efficiency in their filtration of leukocyte at high flow rate, but once again their footprint was significantly larger than ours. Our previous approach using Dean flows[21] demonstrated a 2.5 ml/min flow rate in processing of neuroblastoma and glioma cells but showed only a moderate efficiency (~80%). Similar results were reported by the deformability-based methods, but at a much lower throughput (5–42 μl/min).[50,51] In a sheath-based channel, however, such a low flow rate (and thus throughput) was critical to permit a high 99% efficiency.[52] Thus, in most of the systems reported to date, there is a clear tradeoff between throughput and efficiency, i.e., high filtration efficiency requires low throughput and vice versa. Our device presented herein, however, offers high efficiency while maintaining a relatively high throughput, leading to a more efficient way in processing large sample volumes.

Viability of filtered cells is a critical concern. Compared with other inertial platforms in Table I, our viability results can be further improved and this can be accomplished in a number of ways. First, reducing operational flow rate to $Re = 30$ would reduce shear stress to $\tau_w = 76.8\,\text{dyn/cm}^2$ (i.e., below the $100\,\text{dyn/cm}^2$ critical value). Second, scaling up the channel (increasing w and h in tandem) is not going to affect particle/cell focusing behavior according to our previous work but will substantially reduce the shear stress as $\tau_w \propto D_h^{-3}$. Finally, the size of the outlet channels can be increased in order to minimize fluidic shear in the outlet and thus reduce cell damage.

During our experiments, we observed that cell debris accumulates at the sharp corners of the trifurcating output region (Fig. 7(b)), mainly due to the cell-to-cell interactions and the excessive transient shear stress. This accumulation of cell debris further narrows the channel cross-section and increases fluidic resistance of the central outlet branch. Thus, more cells could exit the channel from side outlets with smaller fluidic resistances, potentially reducing the filtration efficiency. Nevertheless, at $Re = 50$, the fluid drag was sufficiently strong to continually clear this debris through the output. Influence on the efficiency was found to be not significant,

leading to mean values of $\eta = 99\%$. Channel clogging by cell debris can also be overcome by minimizing shear stress through enlargement of the main and the outlet channels or by reducing flow *Re*. Alternatively, surface treatment of channel walls or use of biocompatible materials may help to further prevent nonspecific absorption and mitigate clogging.[53]

Cell deformability has been reported to influence inertial focusing.[51] In our case, this intrinsic property does not affect device performance in terms of filtration efficiency. This is primarily because the deformability-induced drift velocity of cells is in the same direction as the rotation-induced lift force. Both of them drive cells to channel center.[51] As a result, the efficiency of LNCaP cells achieves >99% just as that of rigid particles ($Re = 50$, Figs. 5(b) and 5(c)).

While filtration in high AR channels demonstrated by us[32,33] and others[34] has a similar potential for sample concentration (also purification in processing of complex samples), the design presented herein offers a number of critical advantages. First, our system provides double the enrichment ratio and filtration efficiency in a single-stage as compared to the existing high AR channel designs. The high AR platform comprises two target side outlets and one waste outlet in the center. Hence, for single-stage processing, the concentration enhancement is only 1.5×, which is half of that in our system with the same outlet configuration. In terms of removal of smaller microparticles from complex samples, our device achieves 67% removal rate, which is more effective than the 33% rate of the high AR channels.

Second, sequencing multiple devices has the potential to offer an improved sample concentration performance. Multi-stage processing can exponentially increase the enhancement ratio of concentration and purity, which is $3^n\times$ for n stages in our low AR device. This is in contrast to $1.5^n\times$ for the same number of stages in a conventional high AR microchannel. For instance, sequencing 2 stages would lead to 9× vs. 2.25× enhancement in these devices. Increasing the resistance ratio of the central and side outlets can further enhance the concentration ratio. However, multi-stage sequencing requires careful consideration. Since only a fraction of the input flow exits through the center outlet, each subsequent design will need to be optimized for different flow conditions. In essence, different devices (although similar in design concept) will need to be connected in series. Reusing a single device multiple times, which is the simplest approach to increasing enrichment ratio, will not necessary offer the best results because multiple transfers of the fragile LNCaP and HPET cells can lead to loss in the external connections.

Third, fabrication of low AR microchannels is much easier than that of high AR counterparts. Bhagat *et al.*[28] showed that $AR = 5$ is optimal for processing RBCs; yet it is challenging to fabricate narrow channels with such AR, which is typical in inertial focusing. Even though the channel can be patterned using photolithography, the life time of the master mold for soft lithography or hot embossing is limited due to small adhesion (contact) area between the pattern and the substrate. Indeed, to circumvent this issue, Bhagat *et al.*[28] used a double molding technique involving multiple processes including deep reactive-ion etching (DRIE) of a silicon wafer, which is expensive and time consuming. Conversely, fabrication of low AR channels (e.g., $AR = 0.2$ reported herein) is much simpler and the master molds are much more robust. In addition, low AR channel is more practical to fabricate via mass production techniques such as injection molding.

In summary, we have successfully demonstrated a simple low AR microchannel that can be used for single step filtration and concentration of cellular or particle samples. The low AR nature of the device provides a simple platform with ultra-high efficiency and ease of cascading and paralleling. We envision numerous broader applications in filtration and concentration of cells or particles for sample preparation or purification.

EXPERIMENTAL SECTION

Device fabrication

Microchannels were fabricated using standard soft lithography methods. Briefly, we utilized the dry resist film (PerMX 3050 series, DuPont Electronic Technologies) to pattern masters for microchannels on a 3 in. silicon wafer by conventional photolithography. Polydimethylsiloxane (PDMS, Sylgard 184, Dow Corning) prepolymer was mixed with curing agent in the 10:1 (w/w)

ratio and cast on the master wafer. After a 2-h cure on 80 °C hotplate, the microchannels were replicated in PDMS and bonded with 1 in. × 3 in. glass slides (Fisher Scientific, Inc.) using surface treater (BD-20AC, Electro-Technic Products, Inc.). The inlet and outlet ports were punched manually with a stainless flat-head needle. Topview and sideview images of a single rectangular microchannel were obtained from a pair of microchannels with reciprocal AR. Images captured from a high AR channel (50 μm × 100 μm) represented the sideview of a low AR channel (100 μm × 50 μm). Samples were injected into the device using a syringe pump (NE-1000, New Era Pump Systems, Inc.), with syringe connected to 1/16 in. Peek tubing with fittings (Upchurch Scientific) at device inlet.

Particle suspension

Fluorescent polystyrene beads were used to perform the experiments and measurements to enhance quality of visualization and imaging. To minimize the particle-particle interaction, we diluted bead suspensions with deionized water to reach the VF of 0.025%. For the assessment of filtration efficiency from mixture, we initially mixed 7.32 μm with 20 μm particles in the 1:1 ratio. A small drop (1% v/v) of Tween-20 (Fisher Scientific, Inc.) was added to particle suspensions to minimize clogging. Particles were spiked into diluted human blood (Hoxworth blood center) in saline solution (0.9% NaCl) for cell filtration experiments.

Protocols

The LNCaP human prostate cancer cell line was obtained from American type culture collection and was cultured as described by Pitkänen-Arsiola *et al.*[54] LNCaP cells were grown in 10 cm plates and when they are 80% confluence, the cells are stained with the green fluorescent chloromethyl derivatives of fluorescein diacetate (CMFDA). The cells were stained following manufacturer's protocol (MP02925, Life Technology, Inc.). Briefly, 5 μM CMFDA was diluted in serum free media and added to cells. After 15 min, the media was aspirated and replaced with fresh media; cells were incubated for 45 min. Cells were trypsinized prior to use. Cell viability and growth were determined by counting cell number using trypan blue staining (Sigma Aldrich) and hemocytometer. Approximately 5000 cells were plated in triplicates in 24 well plate and treated with +/− androgen (dihydrotestosterone (DHT)) at concentration of 10^{-8} M. The cells were trypsinized and counted by staining with trypan blue at different time points.

Measurements

To find the focusing length, high-speed images at successive downstream positions were captured using an inverted epi-fluorescence microscope (Olympus IX71) equipped with a 12-bit CCD camera (Retiga EXi, QImaging). 100 frames at each position were captured and stacked using ImageJ® for better visualization and linescans at the same Re. Multiple flow rates ($15 < Re < 175$) were tested to validate the prediction curve in Fig. 3(c). Fluorescent intensity data were obtained from line scan for quantitative assessment of focusing. Fluorescent images in this work were pseudo-colored using ImageJ®. When the mixture of particles was tested, we took images at each channel position alternatively using appropriate filters (fluorescein isothiocyanate (FITC) and 4′,6-Diamidino-2-Phenylindole (DAPI)). The greyscale images from different filters but identical location were merged forming color composite images, which explicitly show the filtration process (Fig. 4 inset). To characterize efficiency and purity, a particle suspension (mixture of 7.32 μm and 20 μm beads) was injected into the low AR channel and samples were collected at each outlet. The samples were then counted using a hemocytometer to determine particle population. Samples were first stirred for 2 min to ensure uniform particle suspension. The particle counting was performed on the microscope stage under fluorescent illumination.

ACKNOWLEDGMENTS

We gratefully acknowledge partial support by the Defense Advanced Research Projects Agency (DARPA) N/MEMS S&T Fundamentals Program under Grant No. N66001-1-4003 issued

by the Space and Naval Warfare Systems Center Pacific (SPAWAR) to the Micro/nano Fluidics Fundamentals Focus (MF3) Center and a grant from the National Institute of Diabetes and Digestive and Kidney Diseases (NIDDK, R01DK060957).

[1]A. Nilsson, F. Petersson, H. Jonsson, and T. Laurell, "Acoustic control of suspended particles in micro fluidic chips," Lab Chip **4**, 131–135 (2004).
[2]G. Agarwal and C. Livermore, "Chip-based size-selective sorting of biological cells using high frequency acoustic excitation," Lab Chip **11**, 2204–2211 (2011).
[3]H.-L. Gou, X.-B. Zhang, N. Bao, J.-J. Xu, X.-H. Xia, and H.-Y. Chen, "Label-free electrical discrimination of cells at normal, apoptotic and necrotic status with a microfluidic device," J. Chromatogr. A **1218**, 5725–5729 (2011).
[4]P. R. Gascoyne, J. Noshari, T. J. Anderson, and F. F. Becker, "Isolation of rare cells from cell mixtures by dielectrophoresis," Electrophoresis **30**, 1388–1398 (2009).
[5]K. Khoshmanesh, S. Baratchi, F. J. Tovar-Lopez, S. Nahavandi, D. Wlodkowic, A. Mitchell, and K. Kalantar-zadeh, "On-chip separation of Lactobacillus bacteria from yeasts using dielectrophoresis," Microfluid. Nanofluid. **12**, 597–606 (2012).
[6]M. A. M. Gijs, "Magnetic bead handling on-chip: New opportunities for analytical applications," Microfluid. Nanofluid. **1**, 22–40 (2004).
[7]M. Zborowski and J. J. Chalmers, "Rare cell separation and analysis by magnetic sorting," Anal. Chem. **83**, 8050–8056 (2011).
[8]Q. Li, J. Li, and X. Hu, in *Proceedings of IEEE NANOMED*, Hong Kong, China (2010), pp. 21–25.
[9]J. Chung, D. Issadore, A. Ullal, K. Lee, R. Weissleder, and H. Lee, "Rare cell isolation and profiling on a hybrid magnetic/size-sorting chip," Biomicrofluidics **7**, 054107 (2013).
[10]S. Li, M. Li, K. Bougot-Robin, W. Cao, I. Yeung Yeung Chau, W. Li, and W. Wen, "High-throughput particle manipulation by hydrodynamic, electrokinetic, and dielectrophoretic effects in an integrated microfluidic chip," Biomicrofluidics **7**, 024106 (2013).
[11]J. DuBose, X. Lu, S. Patel, S. Qian, S. W. Joo, and X. Xuan, "Microfluidic electrical sorting of particles based on shape in a spiral microchannel," Biomicrofluidics **8**, 014101 (2014).
[12]N. Pamme, "Continuous flow separations in microfluidic devices," Lab Chip **7**, 1644–1659 (2007).
[13]J. Zhou and I. Papautsky, "Fundamentals of inertial focusing in microchannels," Lab Chip **13**, 1121–1132 (2013).
[14]G. Segré and A. Silberberg, "Radial particle displacements in Poiseuille flow of suspensions," Nature **189**, 209–210 (1961).
[15]G. Segré and A. Silberberg, "Behaviour of macroscopic rigid spheres in Poiseuille flow," J. Fluid Mech. **14**, 136–157 (1962).
[16]J. P. Matas, V. Glezer, É. Guazzelli, and J. F. Morris, "Trains of particles in finite-Reynolds-number pipe flow," Phys. Fluids **16**, 4192–4195 (2004).
[17]J. P. Matas, J. F. Morris, and É. Guazzelli, "Inertial migration of rigid spherical particles in Poiseuille flow," J. Fluid Mech. **515**, 171–195 (2004).
[18]D. Di Carlo, J. F. Edd, K. J. Humphry, H. A. Stone, and M. Toner, "Particle segregation and dynamics in confined flows," Phys. Rev. Lett. **102**, 094503 (2009).
[19]D. Di Carlo, "Inertial microfluidics," Lab Chip **9**, 3038–3046 (2009).
[20]A. A. S. Bhagat, S. S. Kuntaegowdanahalli, and I. Papautsky, "Continuous particle separation in spiral microchannels using Dean flows and differential migration," Lab Chip **8**, 1906–1914 (2008).
[21]S. S. Kuntaegowdanahalli, A. A. S. Bhagat, G. Kumar, and I. Papautsky, "Inertial microfluidics for continuous particle separation in spiral microchannels," Lab Chip **9**, 2973–2980 (2009).
[22]D. Di Carlo, D. Irimia, R. G. Tompkins, and M. Toner, "Continuous inertial focusing, ordering, and separation of particles in microchannels," Proc. Natl. Acad. Sci. U.S.A. **104**, 18892–18897 (2007).
[23]D. Di Carlo, J. F. Edd, D. Irimia, R. G. Tompkins, and M. Toner, "Equilibrium separation and filtration of particles using differential inertial focusing," Anal. Chem. **80**, 2204–2211 (2008).
[24]A. Russom, A. K. Gupta, S. Nagrath, D. Di Carlo, J. F. Edd, and M. Toner, "Differential inertial focusing of particles in curved low-aspect-ratio microchannels," New J. Phys. **11**, 075025 (2009).
[25]D. R. Gossett, W. M. Weaver, A. J. MacH, S. C. Hur, H. T. K. Tse, W. Lee, H. Amini, and D. Di Carlo, "Label-free cell separation and sorting in microfluidic systems," Anal. Bioanal. Chem. **397**, 3249–3267 (2010).
[26]S. C. Hur, A. J. Mach, and D. Di Carlo, "High-throughput size-based rare cell enrichment using microscale vortices," Biomicrofluidics **5**, 022206 (2011).
[27]W. C. Lee, A. A. S. Bhagat, S. Huang, K. J. Van Vliet, J. Han, and C. T. Lim, "High-throughput cell cycle synchronization using inertial forces in spiral microchannels," Lab Chip **11**, 1359–1367 (2011).
[28]A. A. S. Bhagat, H. W. Hou, L. D. Li, C. T. Lim, and J. Han, "Pinched flow coupled shear-modulated inertial microfluidics for high-throughput rare blood cell separation," Lab Chip **11**, 1870–1878 (2011).
[29]S. Choi, S. Song, C. Choi, and J. K. Park, "Microfluidic self-sorting of mammalian cells to achieve cell cycle synchrony by hydrophoresis," Anal. Chem. **81**, 1964–1968 (2009).
[30]M. G. Lee, S. Choi, and J. K. Park, "Inertial separation in a contraction-expansion array microchannel," J. Chromatogr. A **1218**, 4138–4143 (2011).
[31]M. G. Lee, S. Choi, H. J. Kim, H. K. Lim, J. H. Kim, N. Huh, and J. K. Park, "Inertial blood plasma separation in a contraction-expansion array microchannel," Appl. Phys. Lett. **98**, 253702 (2011).
[32]A. A. S. Bhagat, S. S. Kuntaegowdanahalli, and I. Papautsky, "Enhanced particle filtration in straight microchannels using shear-modulated inertial migration," Phys. Fluids **20**, 101702 (2008).
[33]A. A. S. Bhagat, S. S. Kuntaegowdanahalli, and I. Papautsky, "Inertial microfluidics for continuous particle filtration and extraction," Microfluid. Nanofluid. **7**, 217 (2009).
[34]A. J. Mach and D. Di Carlo, "Continuous scalable blood filtration device using inertial microfluidics," Biotechnol. Bioeng. **107**, 302–311 (2010).

[35]J. Hansson, J. M. Karlsson, T. Haraldsson, H. Brismar, W. Van Der Wijngaart, and A. Russom, "Inertial microfluidics in parallel channels for high-throughput applications," Lab Chip **12**, 4644–4650 (2012).
[36]Å. Pousette, K. Carlström, P. Henriksson, M. Grande, and R. Stege, "Use of a hormone-sensitive (LNCaP) and a hormone-resistant (LNCaP-r) cell line in prostate cancer research," Prostate **31**, 198–203 (1997).
[37]D. G. Bostwick, H. B. Burke, D. Djakiew, S. Euling, S.-m. Ho, J. Landolph, H. Morrison, B. Sonawane, T. Shifflett, D. J. Waters, and B. Timms, "Human prostate cancer risk factors," Cancer **101**, 2371–2490 (2004).
[38]A. M. De Marzo, A. K. Meeker, S. Zha, J. Luo, M. Nakayama, E. A. Platz, W. B. Isaacs, and W. G. Nelson, "Human prostate cancer precursors and pathobiology," Urology **62**, 55–62 (2003).
[39]J. M. Barnes, J. T. Nauseef, and M. D. Henry, "Resistance to fluid shear stress is a conserved biophysical property of malignant cells," PLoS One **7**, e50973 (2012).
[40]A. Gu, J. Yuan, M. Wills, and S. Kasper, "Prostate cancer cells with stem cell characteristics reconstitute the original human tumor *in vivo*," Cancer Res. **67**, 4807–4815 (2007).
[41]S. Kasper, "Exploring the origins of the normal prostate and prostate cancer stem cell," Stem Cell Rev. **4**, 193–201 (2008).
[42]S. Kasper, "Stem cells: The root of prostate cancer?," J. Cell. Physiol. **216**, 332–336 (2008).
[43]A. J. Mach, J. H. Kim, A. Arshi, S. C. Hur, and D. Di Carlo, "Automated cellular sample preparation using a centrifuge-on-a-chip," Lab Chip **11**, 2827–2834 (2011).
[44]J. Warrick, B. Casavant, M. Frisk, and D. Beebe, "A microfluidic cell concentrator," Anal. Chem. **82**, 8320–8326 (2010).
[45]J. Nilsson, M. Evander, B. Hammarström, and T. Laurell, "Review of cell and particle trapping in microfluidic systems," Anal. Chim. Acta **649**, 141–157 (2009).
[46]A. K. Balasubramanian, K. A. Soni, A. Beskok, and S. D. Pillai, "A microfluidic device for continuous capture and concentration of microorganisms from potable water," Lab Chip **7**, 1315–1321 (2007).
[47]Z. Liu, F. Huang, J. Du, W. Shu, H. Feng, X. Xu, and Y. Chen, "Rapid isolation of cancer cells using microfluidic deterministic lateral displacement structure," Biomicrofluidics **7**, 011801 (2013).
[48]E. Sollier, D. E. Go, J. Che, D. R. Gossett, S. O'Byrne, W. M. Weaver, N. Kummer, M. Rettig, J. Goldman, N. Nickols, S. McCloskey, R. P. Kulkarni, and D. Di Carlo, "Size-selective collection of circulating tumor cells using vortex technology," Lab Chip **14**, 63–77 (2014).
[49]L. Wu, G. Guan, H. W. Hou, A. A. S. Bhagat, and J. Han, "Separation of leukocytes from blood using spiral channel with trapezoid cross-section," Anal. Chem. **84**, 9324–9331 (2012).
[50]H. W. Hou, A. A. S. Bhagat, A. G. Chong, P. Mao, K. S. Tan, J. Han, and C. T. Lim, "Deformability based cell margination–A simple microfluidic design for malaria-infected erythrocyte separation," Lab Chip **10**, 2605–2613 (2010).
[51]S. C. Hur, N. K. Henderson-Maclennan, E. R. B. McCabe, and D. Di Carlo, "Deformability-based cell classification and enrichment using inertial microfluidics," Lab Chip **11**, 912–920 (2011).
[52]M. G. Lee, J. H. Shin, C. Y. Bae, S. Choi, and J.-K. Park, "Label-free cancer cell separation from human whole blood using inertial microfluidics at low shear stress," Anal. Chem. **85**, 6213–6218 (2013).
[53]E. K. U. Larsen and N. B. Larsen, "One-step polymer surface modification for minimizing drug, protein, and DNA adsorption in microanalytical systems," Lab Chip **13**, 669–675 (2013).
[54]T. Pitkänen-Arsiola, J. E. Tillman, G. Gu, J. Yuan, R. L. Roberts, M. Wantroba, G. A. Coetzee, M. S. Cookson, and S. Kasper, "Androgen and anti-androgen treatment modulates androgen receptor activity and DJ-1 stability," Prostate **66**, 1177–1193 (2006).
[55]X. Hu, P. H. Bessette, J. Qian, C. D. Meinhart, P. S. Daugherty, and H. T. Soh, "Marker-specific sorting of rare cells using dielectrophoresis," Proc. Natl. Acad. Sci. U. S. A. **102**, 15757–15761 (2005).
[56]S. Shim, K. Stemke-Hale, A. M. Tsimberidou, J. Noshari, T. E. Anderson, and P. R. C. Gascoyne, "Antibody-independent isolation of circulating tumor cells by continuous-flow dielectrophoresis," Biomicrofluidics **7**, 011807 (2013).
[57]C. M. Earhart, C. E. Hughes, R. S. Gaster, C. C. Ooi, R. J. Wilson, L. Y. Zhou, E. W. Humke, L. Xu, D. J. Wong, S. B. Willingham, E. J. Schwartz, I. L. Weissman, S. S. Jeffrey, J. W. Neal, R. Rohatgi, H. A. Wakelee, and S. X. Wang, "Isolation and mutational analysis of circulating tumor cells from lung cancer patients with magnetic sifters and biochips," Lab Chip **14**, 78–88 (2014).
[58]S. Nagrath, L. V. Sequist, S. Maheswaran, D. W. Bell, D. Irimia, L. Ulkus, M. R. Smith, E. L. Kwak, S. Digumarthy, A. Muzikansky, P. Ryan, U. J. Balis, R. G. Tompkins, D. A. Haber, and M. Toner, "Isolation of rare circulating tumor cells in cancer patients by microchip technology," Nature **450**, 1235–1239 (2007).
[59]P. Augustsson, C. Magnusson, M. Nordin, H. Lilja, and T. Laurell, "Microfluidic, label-free enrichment of prostate cancer cells in blood based on acoustophoresis," Anal. Chem. **84**, 7954–7962 (2012).
[60]A. H. J. Yang and H. T. Soh, "Acoustophoretic sorting of viable mammalian cells in a microfluidic device," Anal. Chem. **84**, 10756–10762 (2012).
[61]D. J. Collins, T. Alan, and A. Neild, "Particle separation using virtual deterministic lateral displacement (vDLD)," Lab Chip **14**, 1595–1603 (2014).
[62]T. M. Geislinger and T. Franke, "Sorting of circulating tumor cells (MV3-melanoma) and red blood cells using non-inertial lift," Biomicrofluidics **7**, 044120 (2013).